Supporting Information

Facile Strategy for Obtaining Luminescent Polymorphs Based on Chirality of Boron-Fused Azomethine Complex

Shunsuke Ohtani, Yusuke Takeda, Masayuki Gon, Kazuo Tanaka* and Yoshiki Chujo

Department of Polymer Chemistry, Graduate School of Engineering, Kyoto University Katsura, Nishikyo-ku, Kyoto 615-8510, Japan

E-mail: tanaka@poly.synchem.kyoto-u.ac.jp

Contents:

General

^{1}H (400 MHz), ^{13}C (100 MHz) ^{11}B (128 MHz) NMR spectra were recorded on JEOL JNM-AL400 or JNM-EX400 spectrometers. Samples were analyzed in $CDCl_3$ and DMSO-d_6. The chemical shift values were expressed relative to tetramethylsilane (TMS) for ^{1}H and ^{13}C NMR as an internal standard in $CDCl_3$ and $BF_3 \cdot OEt_2$ for ^{11}B NMR as a capillary standard. Analytical thin-layer chromatography (TLC) was performed with silica gel 60 Merck F254 plates. Column chromatography was performed with Wakogel® C-300 silica gel. High-resolution mass (HRMS) spectrometry was performed at the Technical Support Office (Department of Synthetic Chemistry and Biological Chemistry, Graduate School of Engineering, Kyoto University), and the HRMS spectra were obtained on a Thermo Fisher Scientific EXACTIVE spectrometer for electrospray ionization (ESI). UV–vis–NIR absorption spectra were recorded on a SHIMADZU UV-3600 spectrophotometer, and samples were analyzed at room temperature. Photoluminescence (PL) spectra were measured on a HORIBA JOBIN YVON Fluoromax-4P spectrofluorometer. Absolute PL quantum efficiency was measured on a Hamamatsu Photonics Quantaurus-QY Plus C13534-01. The PL lifetime measurement was performed on a Horiba FluoroCube spectrofluorometer system; excitation was carried out using a UV diode laser (NanoLED 375 nm). X-ray crystallographic analysis was carried out by Rigaku R-AXIS RAPID-F imaging plate diffractometer with graphite-monochromated MoKα radiation and Rigaku Saturn 724+ with MicroMax-007HF CCD diffractometer with Varimax Mo optics using graphite-monochromated MoKα radiation. The analysis was carried out with direct methods (SHELX-2014/7) using Yadokari-XG. The program Mercury 3.3.1 was used to generate the X-ray structural diagram. Thermogravimetric analyses (TGA) were recorded on a Hitachi High-Tech Science Corp. STA7200RV. Differential scanning calorimetry (DSC) was recorded on a Hitachi High-Tech Science Corp. DSC7020. Circular dichroism (CD) spectra were measured on a JASCO J-820 spectropolarimeter. Circularly polarized luminescence (CPL) spectra were recorded on a JASCO CPL-200S spectrofluoropolarimeter. Solid-state CPL spectra were measured for (*R*)- and (*S*)-**BAmCl** (0.5 mg) mixed with KBr (150 mg). Tablets (diameter: 10 mm, (*R*)- or (*S*)-**BAmCl** /KBr) were prepared using a tablet forming machine (48.2 kN, press time: 3 min). Chiral high performance liquid chromatography (HPLC) was performed with YMC CHIRAL ART Amylose-SA (5μm) 250×20 mmI.D. and SHIMADZU Prominence Modular HPLC system. Specific rotations ($[\alpha]^{t}_{D}$) were measured with a Rudolph Research AUTOPOL IV Automatic Polarimeter.

Materials

Commercially available compounds used without purification:

2-Amino-5-chlorophenol (Tokyo Chemical Industry Co, Ltd.)

4-(Diethylamino)salicylaldehyde (Tokyo Chemical Industry Co, Ltd.)

Boron trifluoride diethyl etherate (≥46% BF_3 basis) ($BF_3 \cdot OEt_2$) (Sigma-Aldrich Co. LLC.)

Commercially available solvents:

EtOH (Wako Pure Chemical Industries, Ltd.), $CHCl_3$ (Wako Pure Chemical Industries, Ltd.), *n*-hexane (Wako Pure Chemical Industries, Ltd.) and CH_2Cl_2 (Wako Pure Chemical Industries, Ltd.) were used without further purification. Deoxidized grade toluene (Wako Pure Chemical Industries, Ltd.) were used without further purification. Triethylamine (Kanto Chemical Co., Inc.) was purified by passage through solvent purification columns under argon pressure.

Synthetic Procedures and Characterization

Synthesis of AmCl

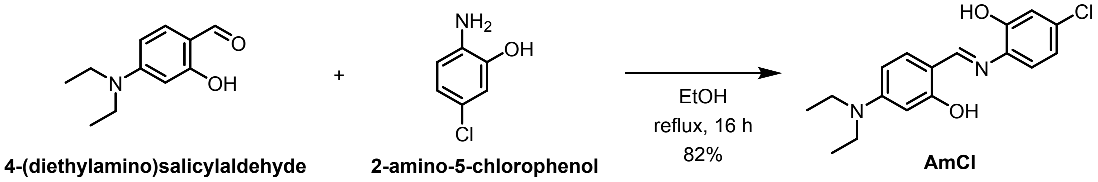

Scheme S1. Synthesis of **AmCl**.

2-Amino-5-chlorophenol (0.37 g, 2.59 mmol) was dissolved in 20 mL of EtOH. 4-(Diethylamino)salicylaldehyde (0.50 g, 2.59 mmol) was added to the solution and the reaction mixture was stirred at reflux temperature for 16 h. During course of the reaction, the product was precipitated from the reaction mixture. After cooling to room temperature, the resulting mixture was poured into water. The precipitation collected by filtration was dried *in vacuo* to give **AmCl** as an orange solid (0.68 g, 82%). ^{1}H NMR ($CDCl_3$, 400 MHz), δ (ppm): 8.40 (s, 1H), 7.19 (d, J = 8.8 Hz, 1H), 7.00−6.98 (m, 2H), 6.89 (dd, J = 8.3, 2.2 Hz, 1H), 6.28 (dd, J = 8.8, 2.4 Hz, 1H), 6.19 (d, J = 2.4 Hz, 1H), 3.42 (q, J = 7.1 Hz, 4H), 1.22 (t, J = 7.1 Hz, 6H). ^{13}C NMR (DMSO-d_6, 100 MHz), δ (ppm): 164.5, 159.8, 151.6, 151.2, 134.6, 133.9, 129.4, 119.9, 119.3, 115.8, 108.9, 103.7, 97.0, 43.8, 12.5. HRMS (ESI): Calcd for $[M+H]^+$, 319.1208; Found, m/z 319.1203. Elemental analysis calcd. for $C_{17}H_{19}ClN_2O_2$: C, 64.05; H, 6.01; N, 8.79. Found: C, 64.10; H, 5.91; N, 8.89.

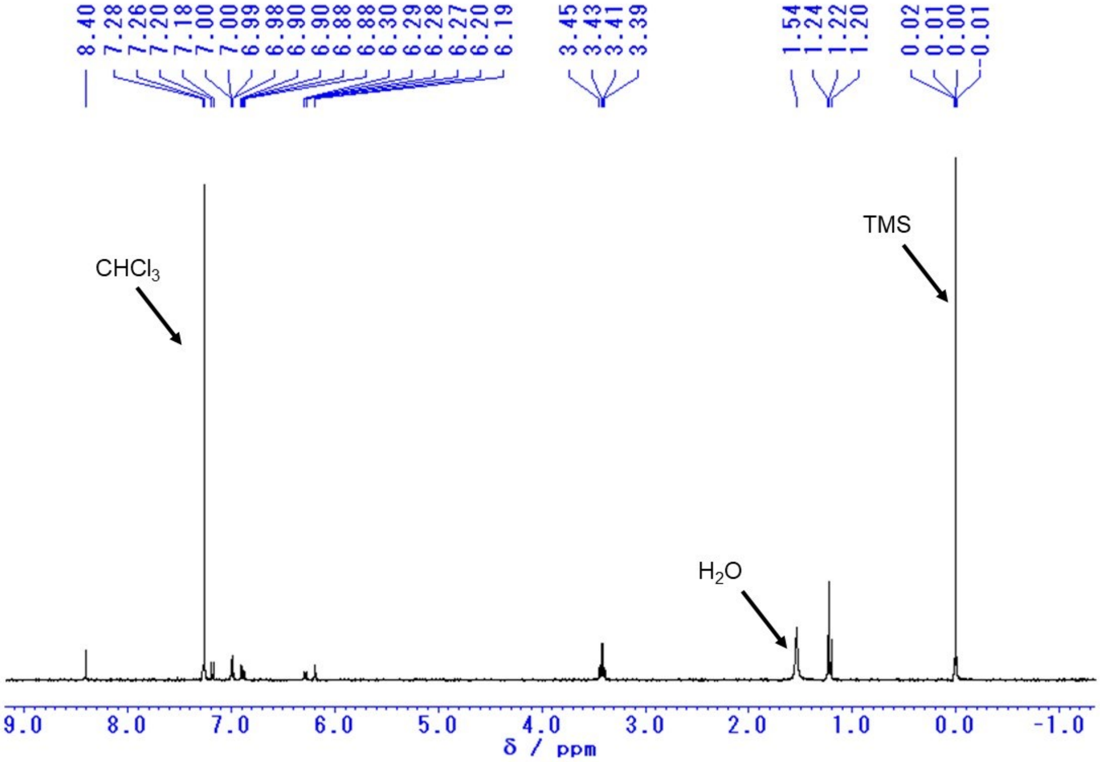

Fig. S1. ^{1}H NMR spectrum of **AmCl**, $CDCl_3$, 400 MHz.

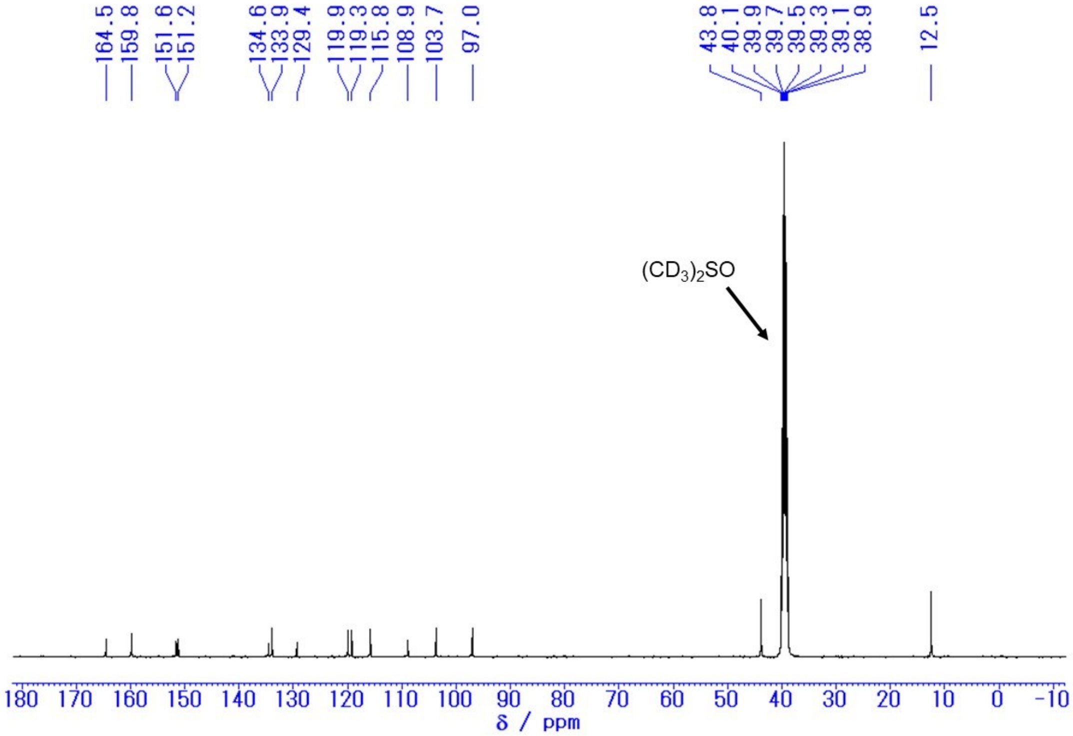

Fig. S2. ^{13}C NMR spectrum of **AmCl**, DMSO-d_6, 100 MHz.

Synthesis of BAmCl

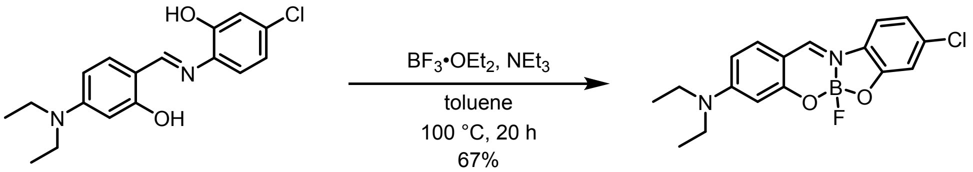

Scheme S2. Synthesis of **BAmCl**.

Am-Cl (0.40 g, 1.25 mmol) was dissolved in 13 mL of dry toluene under Ar atmosphere at room temperature and triethylamine (4 mL) was then added to the solution. $BF_3 \cdot OEt_2$ (3 mL) was added dropwise to the solution and the reaction mixture was stirred at 100 °C for 20 h. After cooling to room temperature, the resulting mixture was quenched by EtOH and concentrated by a rotary evaporator. The residue was purified by chromatography on silica gel with CH_2Cl_2 and dissolved in small amount of $CHCl_3$, and the product was reprecipitated from hexane to give **BAmCl** as an orange solid (0.29 g, 67%). R_f = 0.79 (CH_2Cl_2). HRMS (ESI): Calcd for $[M+Na]^+$, 347.1128; Found, m/z 347.1121. Elemental analysis calcd. for $C_{17}H_{17}BClFN_2O_2$: C, 58.91; H, 4.94; N, 8.08. Found: C, 58.84; H, 4.94; N, 8.07.

Racemic **BAmCl**:

^1H NMR ($CDCl_3$, 400 MHz), δ (ppm): 8.25 (s, 1H), 7.31 (d, J = 9.3 Hz, 1H), 7.22 (d, J = 8.3 Hz, 1H), 7.06 (d, J = 2.0 Hz,1H), 6.86 (dd, J = 8.4, 2.0 Hz, 1H), 6.43 (dd, J = 9.1, 2.5 Hz, 1H), 6.37 (d, J = 2.4 Hz, 1H), 3.47 (m, 4H), 1.25 (t, J = 7.1 Hz, 6H). ^{11}B NMR ($CDCl_3$, 128 MHz), δ (ppm): 4.27 (d, J = 38 MHz). ^{13}C NMR ($CDCl_3$, 100 MHz), δ (ppm): 160.1, 156.4, 155.9, 148.1, 133.8, 133.4, 129.5, 119.4, 114.7, 113.4, 108.6, 107.4, 99.5, 45.2, 12.7.

Enantiomeric **BAmCl-fr1** ((*R*)-**BAmCl**):

$[\alpha]^{23}_D = +1226.5$ (c 0.1, $CHCl_3$)

^1H NMR ($CDCl_3$, 400 MHz), δ (ppm): 8.25 (s, 1H), 7.31 (d, J = 9.0 Hz, 1H), 7.22 (d, J = 8.3 Hz, 1H), 7.06 (d, J = 1.9 Hz, 1H), 6.87 (dd, J = 8.6, 2.2 Hz, 1H), 6.44 (dd, J = 9.0, 2.4 Hz, 1H), 6.37 (d, J = 2.4 Hz, 1H), 3.47 (m, 4H), 1.25 (t, J = 7.1 Hz, 6H). ^{11}B NMR ($CDCl_3$, 128 MHz), δ (ppm): 4.27 (d, J = 38 MHz). ^{13}C NMR ($CDCl_3$, 100 MHz), δ (ppm): 160.1, 156.4, 155.9, 148.0, 133.9, 133.4, 129.5, 119.4, 114.7, 113.4, 108.7, 107.4, 99.6, 45.2, 12.7.

Enantiomeric **BAmCl-fr2** ((*S*)-**BAmCl**):

$[\alpha]^{23}_D = -1244.6$ (c 0.1, $CHCl_3$)

The NMR spectra of **BAmCl-fr2** were the same with **BAmCl-fr1**.

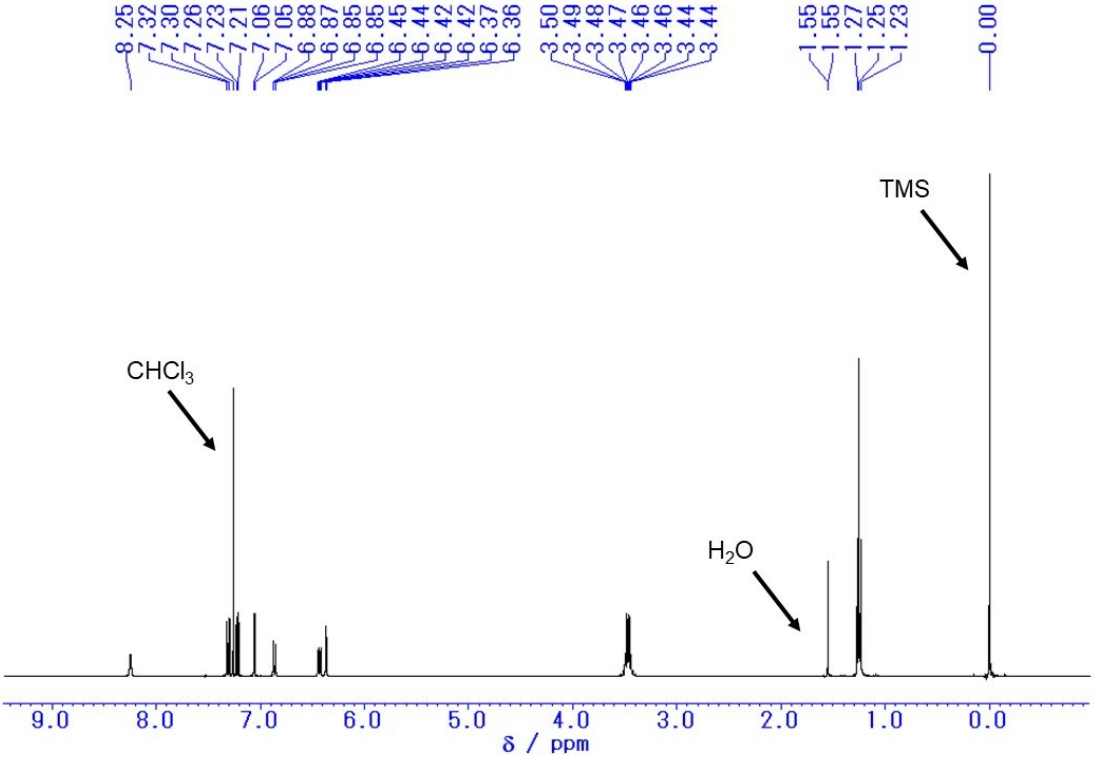

Fig. S3. ^{1}H NMR spectrum of racemic **BAmCl**, $CDCl_3$, 400 MHz.

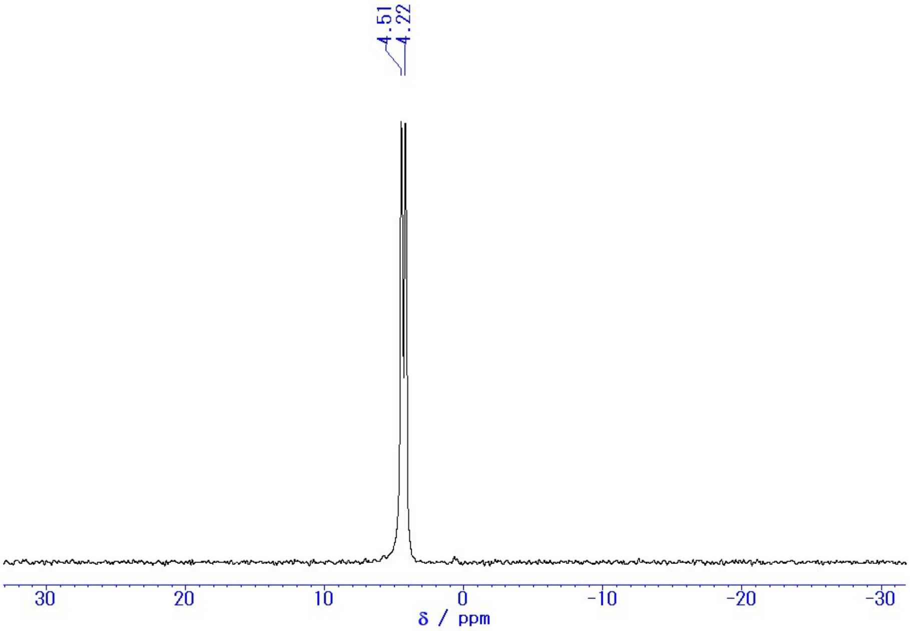

Fig. S4. ^{11}B NMR spectrum of racemic **BAmCl**, $CDCl_3$, 128 MHz.

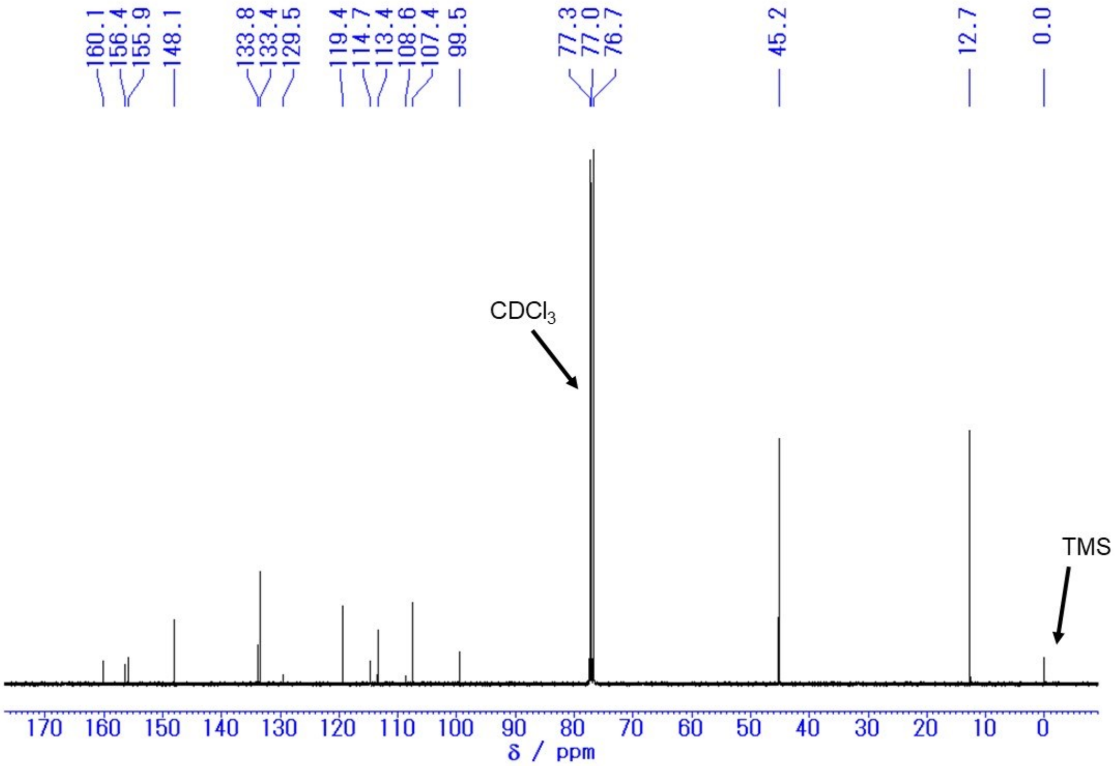

Fig. S5. ^{13}C NMR spectrum of racemic **BAmCl**, $CDCl_3$, 100 MHz.

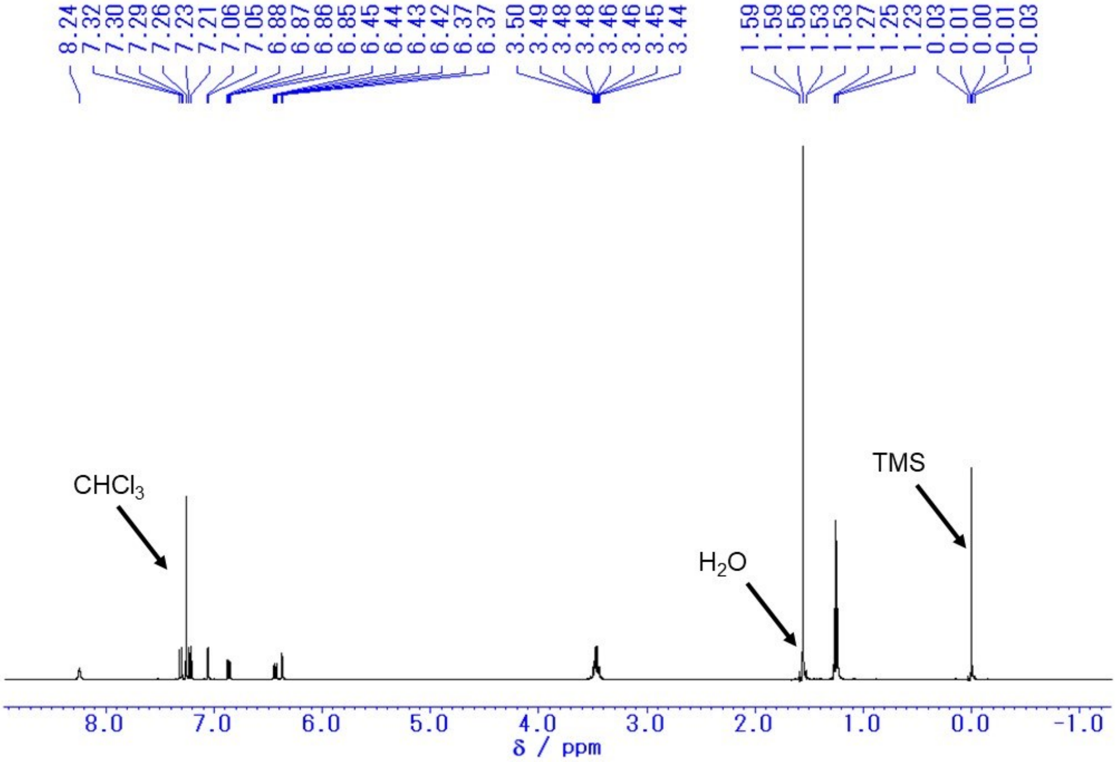

Fig. S6. ^{1}H NMR spectrum of enantiomeric **BAmCl-fr1** ((*R*)-**BAmCl**), $CDCl_3$, 400 MHz.

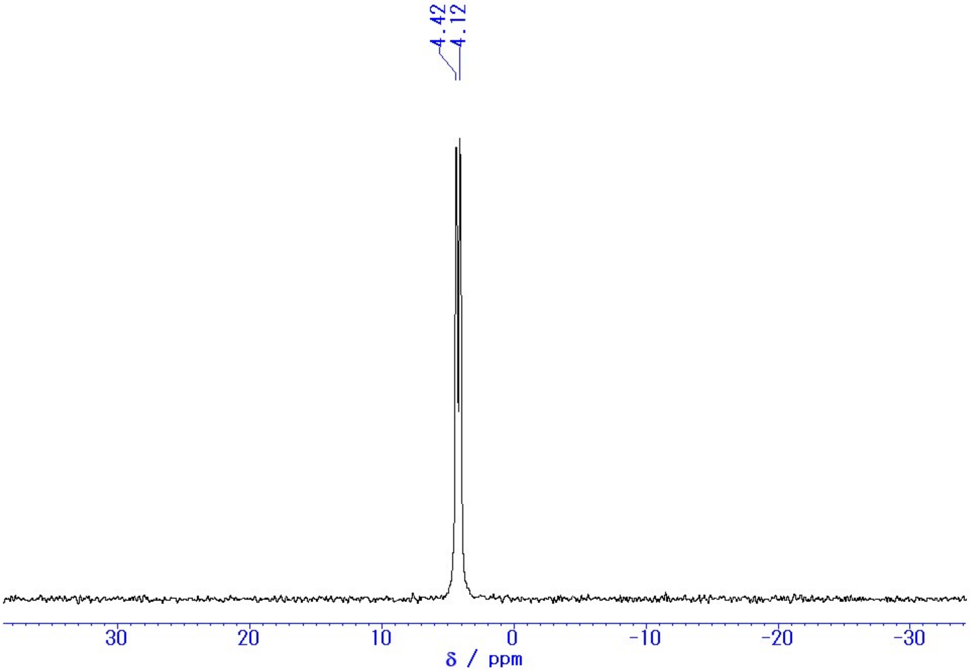

Fig. S7. ^{11}B NMR spectrum of enantiomeric **BAmCl-fr1** ((*R*)-**BAmCl**), $CDCl_3$, 128 MHz.

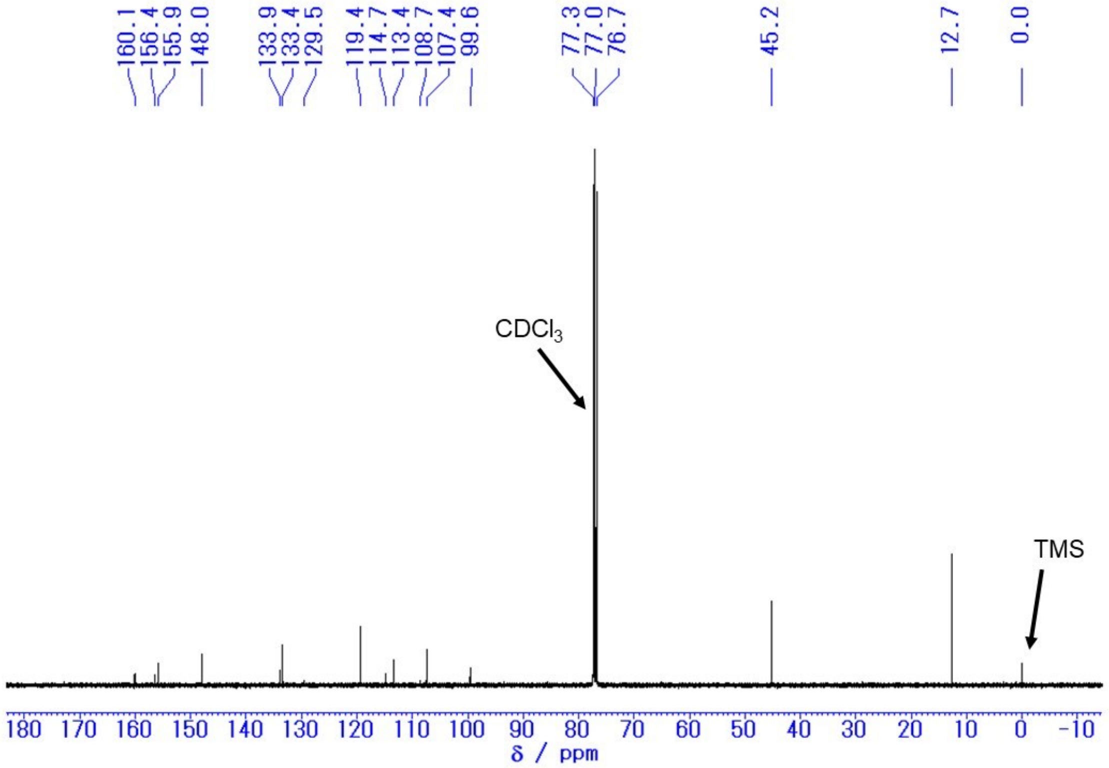

Fig. S8. ^{13}C NMR spectrum of enantiomeric **BAmCl-fr1** ((*R*)**-BAmCl**), CDCl$_3$, 100 MHz.

Chiral resolution of racemate BAmCl

Table S1. Analysis condition of resolution by chiral HPLC

Column	YMC CHIRAL ART Amylose-SA (5 μm) 250 × 20 mmI.D.
Eluent	*n*-hexane/THF (v/v = 1/3)
Flow rate	3.5 mL/min
Detection	UV at 250 nm
Injection	3.0 mL (6.7 mg/mL)
Retention Time	(*R*)-**BAmCl**: 57.2 min. (*S*)-**BAmCl**: 62.6 min.

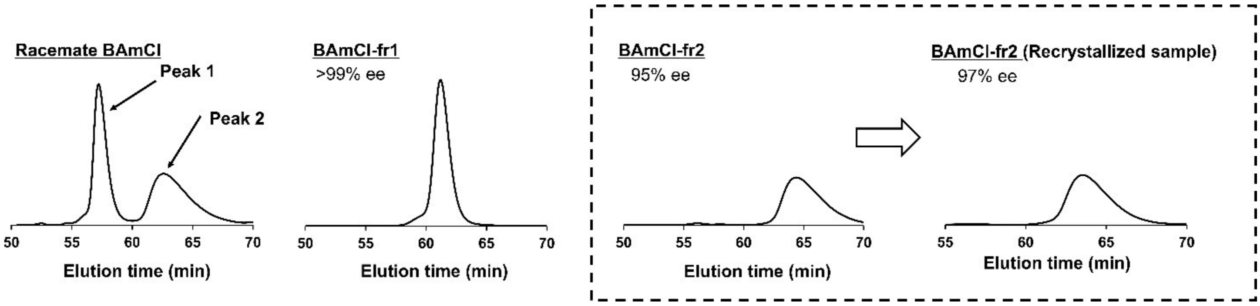

Fig. S9. Chiral HPLC profiles (*n*-hexane/THF 1/3 (v/v), UV/vis absorption detection at 250 nm) of compound **BAmCl**.

Circular dichroism (CD) study

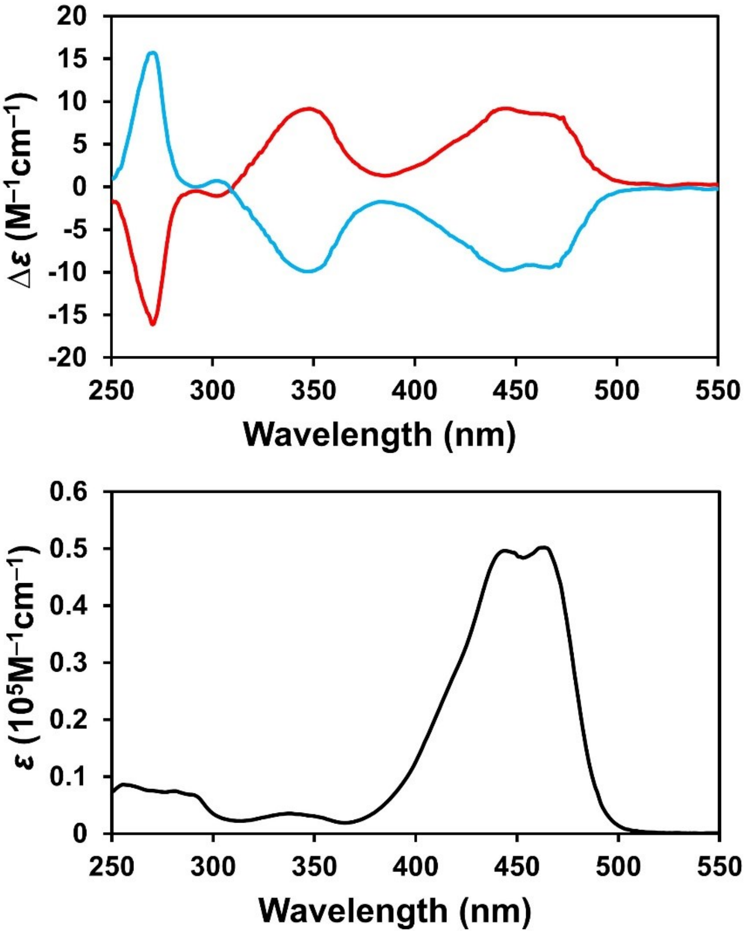

Fig. S10. Circular dichroism (CD) and UV–vis absorption spectra of 2.0×10^{-5} M chloroform solutions containing **BAmCl-fr1** (red) and **BAmCl-fr2** (blue).

Time-dependent circular dichroism (CD) study

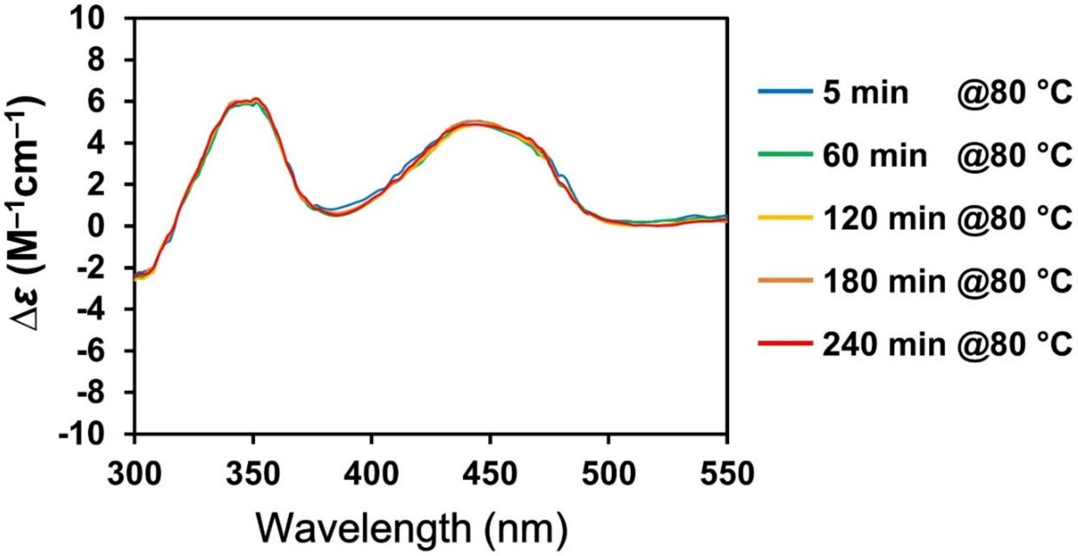

Fig. S11. Time-dependent circular dichroism (CD) spectra of **BAmCl-fr1** ((*R*)-**BAmCl**) in toluene solution (2.0×10^{-5} M) at 80 °C.

X-ray crystal structure analysis of *rac*-BAmCl

Intensity data were collected on a Rigaku R-AXIS RAPID imaging plate area detector with graphite monochromated MoKα radiation (λ = 0.71069 Å). The structures were solved and refined by full-matrix least-squares procedures based on F^2 (SHELXL-2014/7).

Single-crystal of *rac*-**BAmCl** was prepared by vapor diffusion method from $CHCl_3$ solution under hexane atmosphere at room temperature.

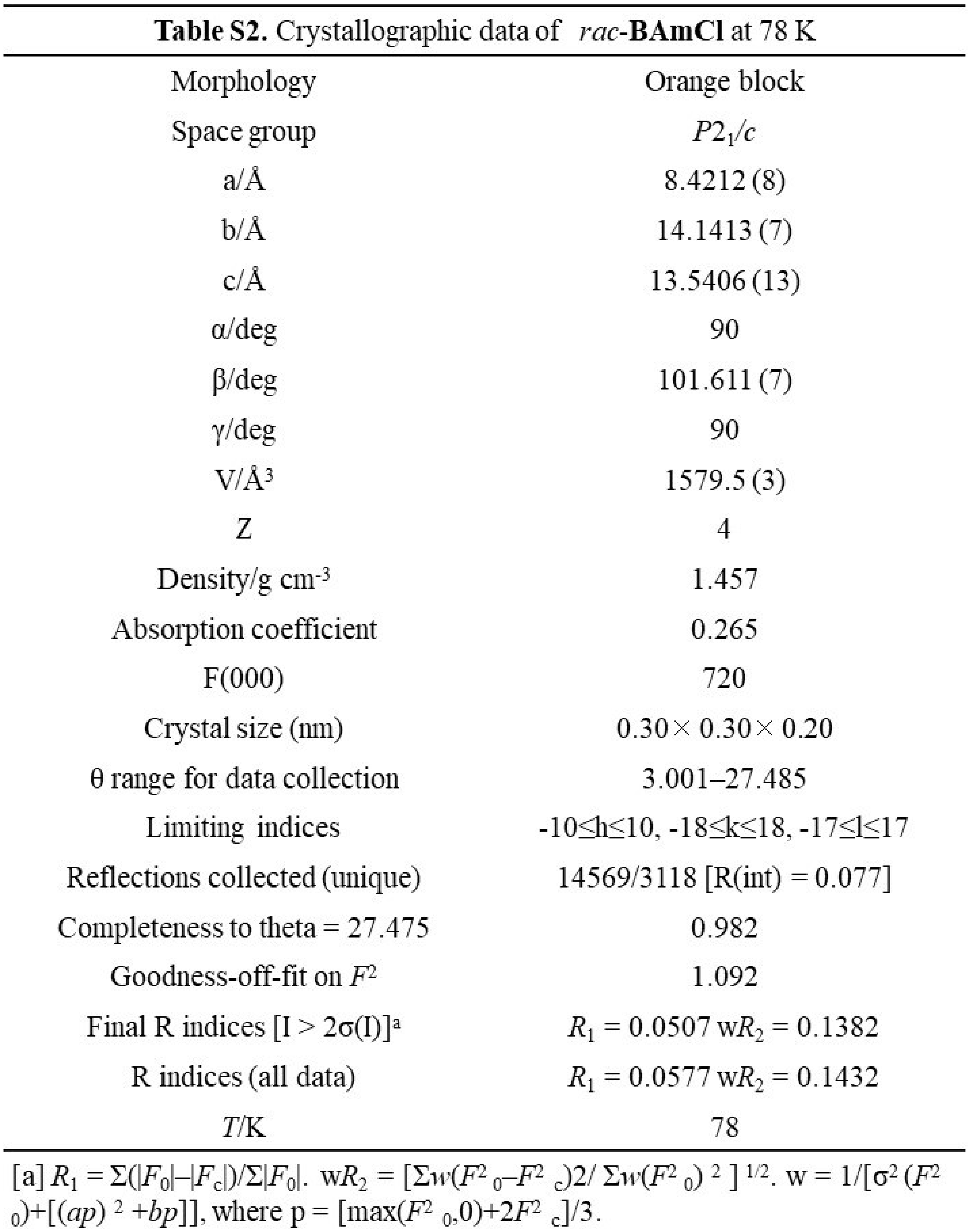

Table S2. Crystallographic data of *rac*-**BAmCl** at 78 K

Morphology	Orange block
Space group	$P2_1/c$
a/Å	8.4212 (8)
b/Å	14.1413 (7)
c/Å	13.5406 (13)
α/deg	90
β/deg	101.611 (7)
γ/deg	90
V/Å^3	1579.5 (3)
Z	4
Density/g cm^{-3}	1.457
Absorption coefficient	0.265
F(000)	720
Crystal size (nm)	0.30× 0.30× 0.20
θ range for data collection	3.001–27.485
Limiting indices	-10≤h≤10, -18≤k≤18, -17≤l≤17
Reflections collected (unique)	14569/3118 [R(int) = 0.077]
Completeness to theta = 27.475	0.982
Goodness-off-fit on F^2	1.092
Final R indices [I > 2σ(I)][a]	R_1 = 0.0507 wR_2 = 0.1382
R indices (all data)	R_1 = 0.0577 wR_2 = 0.1432
T/K	78

[a] $R_1 = \Sigma(|F_0|-|F_c|)/\Sigma|F_0|$. $wR_2 = [\Sigma w(F^2{}_0-F^2{}_c)2/ \Sigma w(F^2{}_0)^2]^{1/2}$. $w = 1/[\sigma^2(F^2{}_0)+[(ap)^2+bp]]$, where $p = [\max(F^2{}_0,0)+2F^2{}_c]/3$.

a) **CH···F interaction**

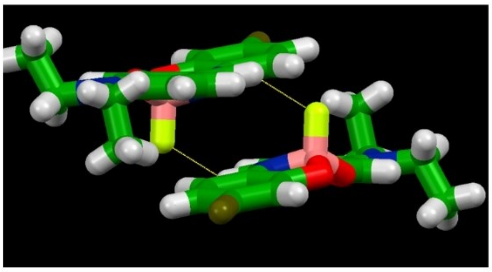

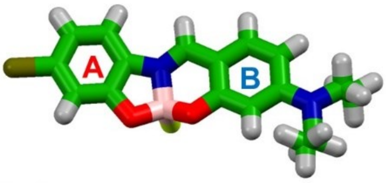

b) **CH···π interaction**

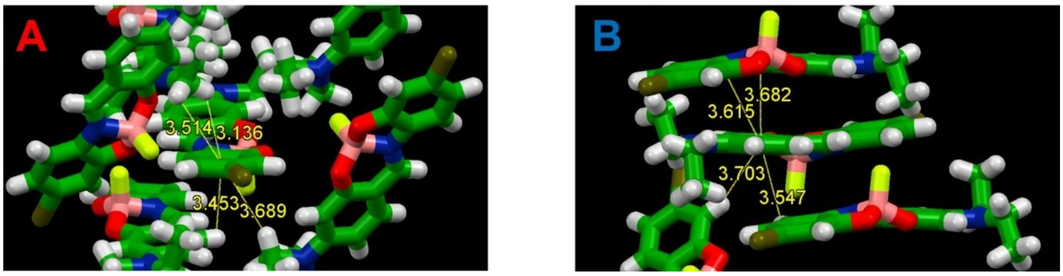

Fig. S12. Intermolecular interaction patterns of *rac*-**BAmCl**. a) CH···F interaction b) CH···π interaction between hydrogen atoms and aromatic rings A or B.

X-ray crystal structure analysis of (*R*)-BAmCl

Intensity data were collected on a Rigaku Saturn 724+ with MicroMax-007HF CCD diffractometer with Varimax Mo optics using graphite-monochromated MoKα radiation. The structures were solved and refined by full-matrix least-squares procedures based on F^2 (SHELXL-2014/7).

Single-crystal of (*R*)-**BAmCl** was prepared by vapor diffusion method from THF solution under hexane atmosphere at room temperature.

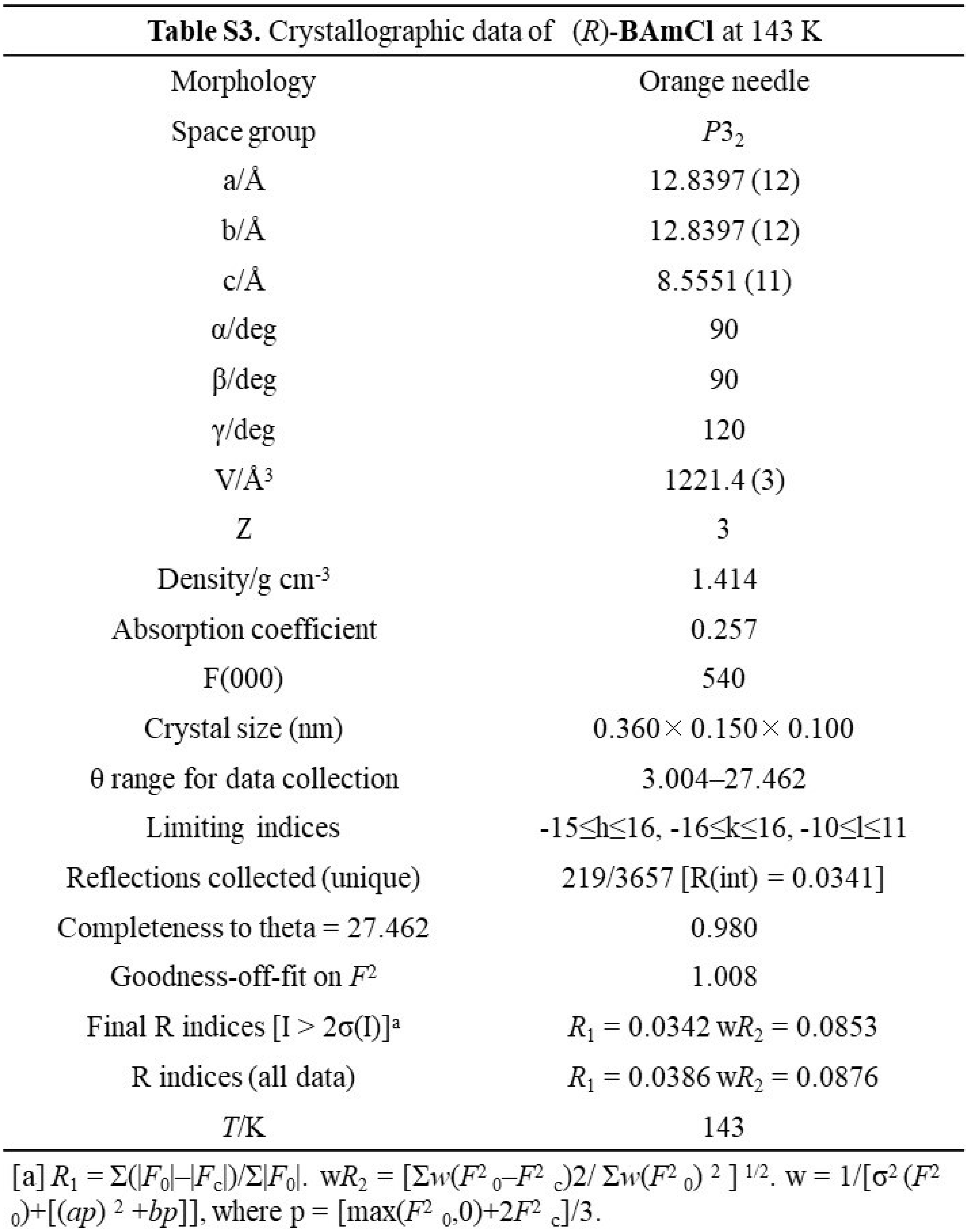

Table S3. Crystallographic data of (*R*)-**BAmCl** at 143 K

Morphology	Orange needle
Space group	$P3_2$
a/Å	12.8397 (12)
b/Å	12.8397 (12)
c/Å	8.5551 (11)
α/deg	90
β/deg	90
γ/deg	120
V/Å^3	1221.4 (3)
Z	3
Density/g cm^{-3}	1.414
Absorption coefficient	0.257
F(000)	540
Crystal size (nm)	0.360 × 0.150 × 0.100
θ range for data collection	3.004–27.462
Limiting indices	-15≤h≤16, -16≤k≤16, -10≤l≤11
Reflections collected (unique)	219/3657 [R(int) = 0.0341]
Completeness to theta = 27.462	0.980
Goodness-off-fit on F^2	1.008
Final R indices [I > 2σ(I)]^a	R_1 = 0.0342 wR_2 = 0.0853
R indices (all data)	R_1 = 0.0386 wR_2 = 0.0876
T/K	143

[a] $R_1 = \Sigma(|F_0|–|F_c|)/\Sigma|F_0|$. w$R_2$ = $[\Sigma w(F^2{}_0–F^2{}_c)2/ \Sigma w(F^2{}_0)^2]^{1/2}$. w = $1/[\sigma^2(F^2{}_0)+[(ap)^2+bp]]$, where p = $[\max(F^2{}_0,0)+2F^2{}_c]/3$.

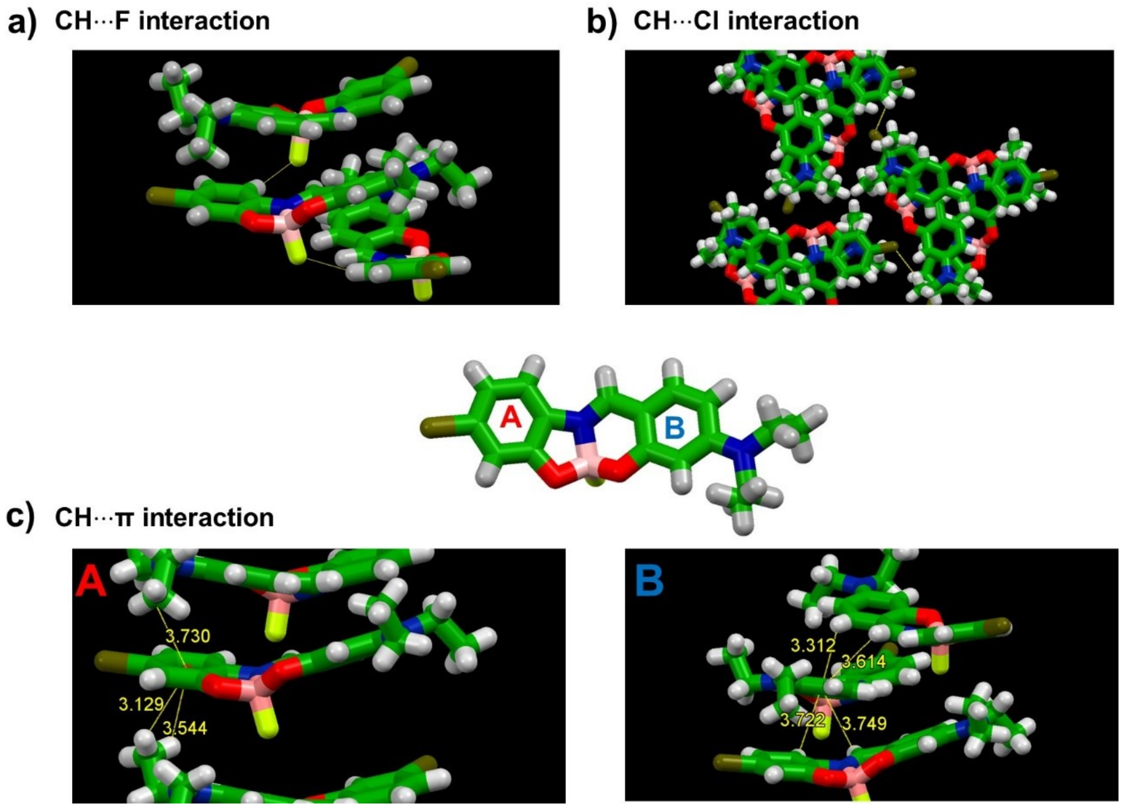

Fig. S13. Intermolecular interaction patterns of (*R*)-**BAmCl**. a) CH···F interaction b) CH···Cl interaction c) CH···π interaction between hydrogen atoms and aromatic rings A or B.

PL lifetime decay curves

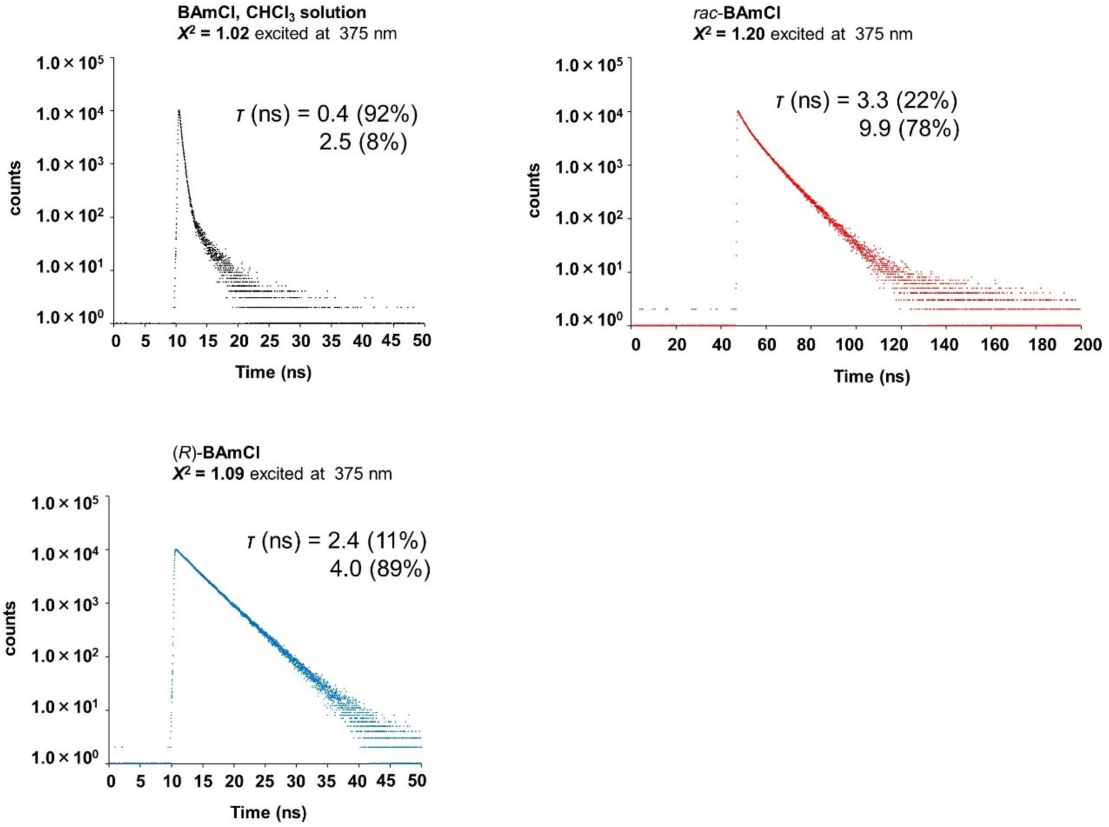

Fig. S14. PL lifetime decay curves of **BAmCl** in chroloform solution (1.0×10^{-5} M) and crystalline states *rac*-**BAmCl** and (*R*)-**BAmCl** at room temperature. Their emissions at the PL peak tops were monitored.

Thermogravimetric analysis (TGA)

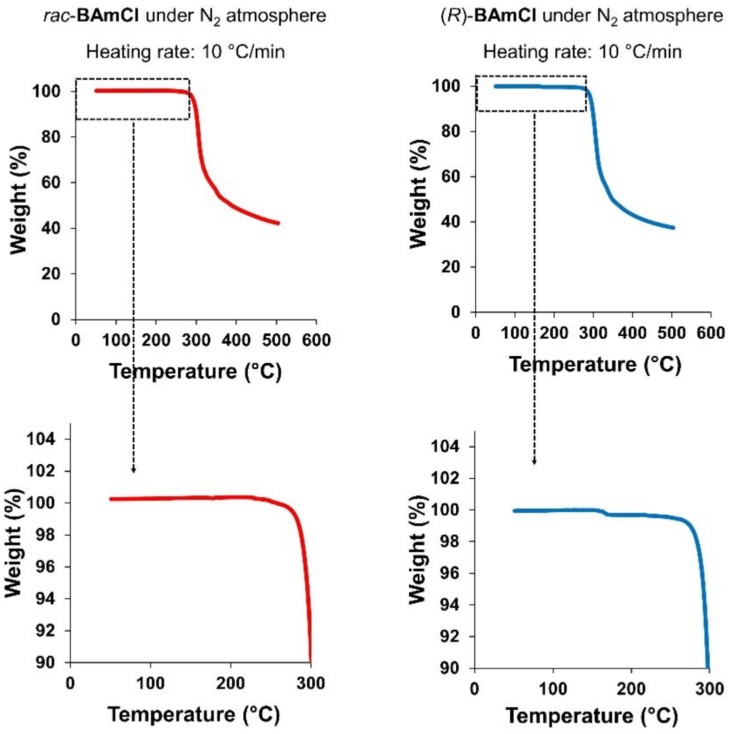

Fig. S15. Thermogravimetric analyses (TGA) curves of *rac*-**BAmCl**, (*R*)-**BAmCl** and (*S*)-**BAmCl**.

We investigated about the initial mass loss in TGA curve of (*R*)-**BAmCl** by using ^{1}H NMR measurement (Figure S15). After heating at 180 °C for 20 min, (*R*)-**BAmCl** showed several peaks in aromatic region of ^{1}H NMR. Therefore, we concluded that the initial mass loss was not related to the sublimation or impurity, but to the decomposition of (*R*)-**BAmCl**.

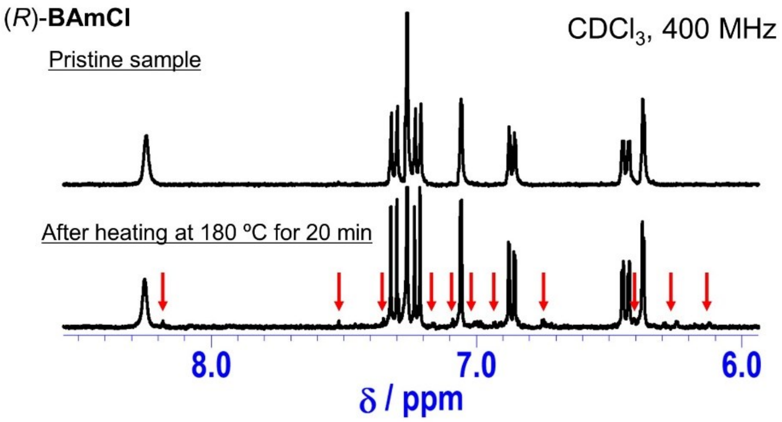

Fig. S16. ^{1}H NMR spectra of pristine and heated (*R*)-**BAmCl** crystalline sample.

Differential scanning calorimetric (DSC) analysis

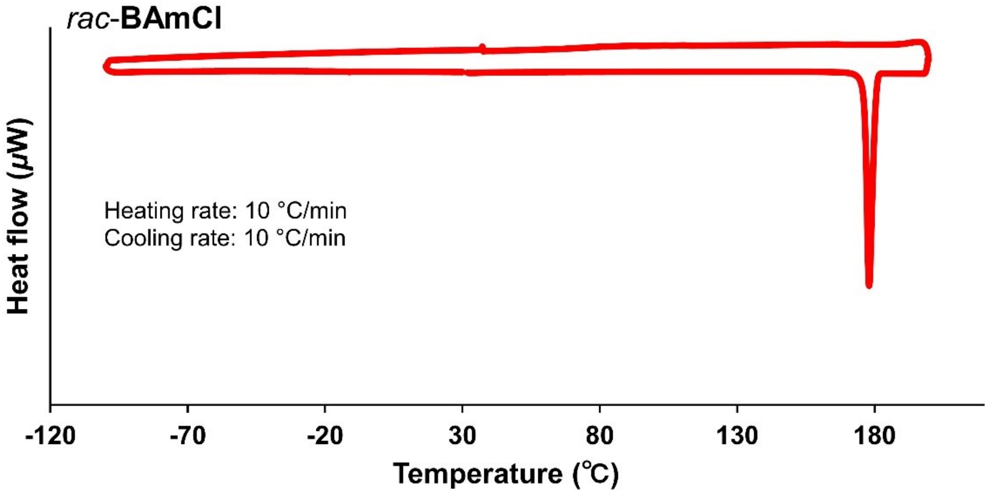

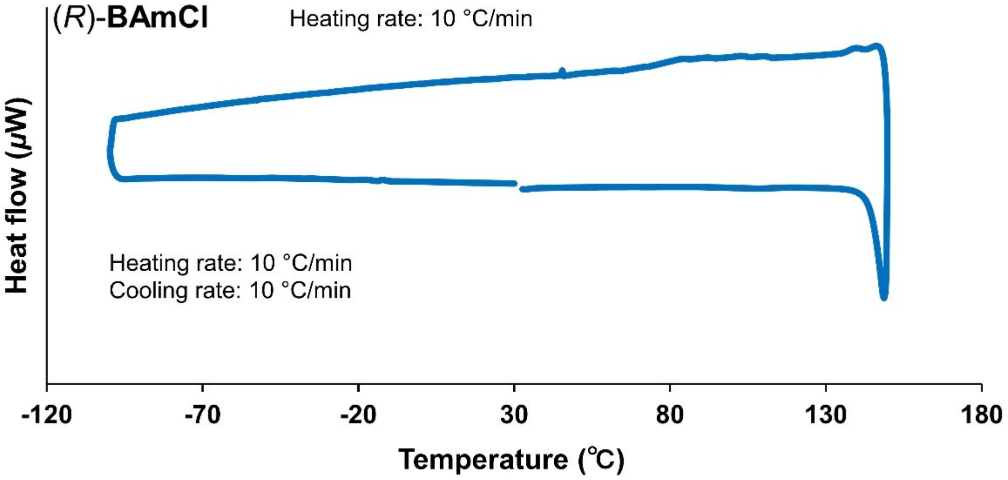

Fig. S17. Differential scanning calorimetric (DSC) curves of *rac*-**BAmCl** and (*R*)-**BAmCl**.

Racemization study of (*R*)-BAmCl

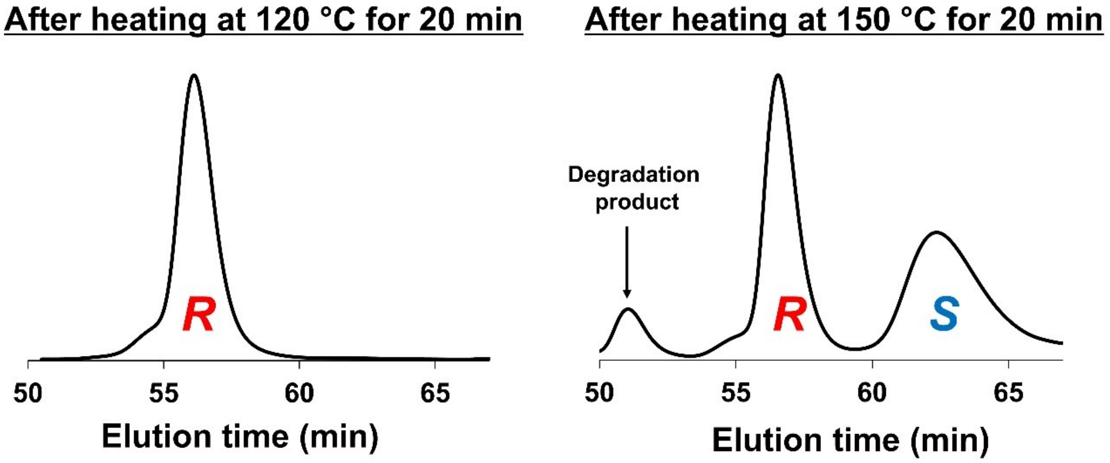

Fig. S18. Chiral HPLC chromatograms (*n*-hexane/THF 1/3 (v/v), UV/vis absorption detection at 250 nm) of crystalline sample (*R*)-**BAmCl**.

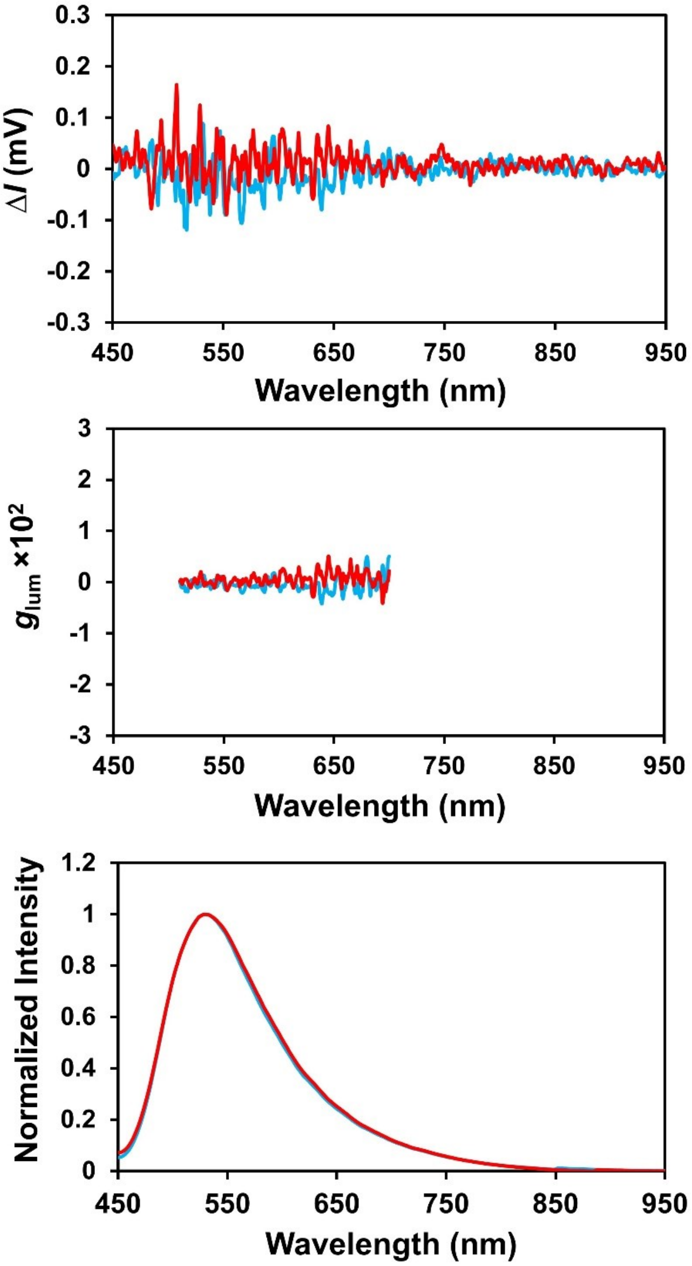

Fig. S19. CPL (top), g_{lum} (middle), and PL (bottom) spectra of (*R*)-**BAmCl** (red) and (*S*)-**BAmCl** (blue) $CHCl_3$ solution (1.0×10^{-4} M) excited at 350 nm.

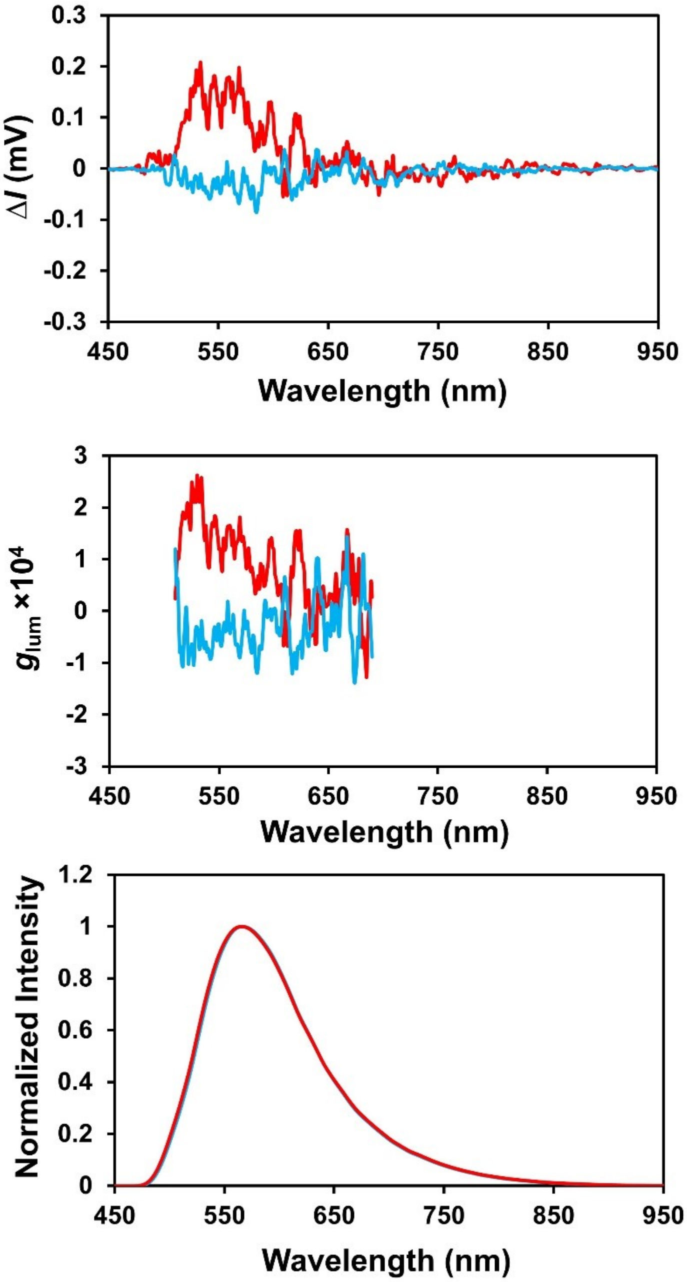

Fig. S20. CPL (top), g_{lum} (middle), and PL (bottom) spectra of (*R*)-**BAmCl** (red) and (*S*)-**BAmCl** (blue) crystalline sample excited at 400 nm.